BNL-113598-2017-JA

Controlling the Growth of Au on Icosahedral Seeds of Pd by Manipulating the Reduction Kinetics

Tian Lv, Xuan Yang, Yiqun Zheng, Hongwen Huang, Lei Zhang, Jing Tao, Likun Pan, and Younan Xia

Submitted to Journal of Physical Chemiistry C

September 2016

Condensed Matter Physics and Materials Science Department

Brookhaven National Laboratory

U.S. Department of Energy
USDOE Office of Science (SC),
Basic Energy Sciences (BES) (SC-22)

DISCLAIMER

Controlling the Growth of Au on Icosahedral Seeds of Pd by Manipulating the Reduction Kinetics

Tian Lv,[†,‡] Xuan Yang,[†] Yiqun Zheng,[§] Hongwen Huang,[†] Lei Zhang,[†] Jing Tao,[¶] Likun Pan,[‡] and Younan Xia[*,†,§]

[†]The Wallace H. Coulter Department of Biomedical Engineering, Georgia Institute of Technology and Emory University, Atlanta, Georgia 30332, United States

[‡]Engineering Research Center for Nanophotonics and Advanced Instrument, Ministry of Education, Department of Physics, East China Normal University, Shanghai 200062, People's Republic of China

[§]School of Chemistry and Biochemistry and School of Chemical and Biomolecular Engineering, Georgia Institute of Technology, Atlanta, Georgia 30332, United States

[¶]Condensed Matter Physics and Materials Science Department, Brookhaven National Laboratory, Upton, New York 11973, United States

*Correspondence author: younan.xia@bme.gatech.edu

ABSTRACT

This article reports a systematic study of how Au atoms nucleate and grow from Pd icosahedral seeds with a multiply twinned structure. By manipulating the reduction kinetics, we obtained Pd−Au bimetallic nanocrystals with two distinct shapes and structures. Specifically, Pd@Au core−shell icosahedra were formed when a relatively fast reduction rate was used for the $HAuCl_4$ precursor. At a slow reduction rate, in contrast, the nucleation and growth of Au atoms were mainly confined to one of the vertices of a Pd icosahedral seed, resulting in the formation of a Au icosahedron by sharing five adjacent faces with the Pd seed. The same growth pattern was observed for Pd icosahedral seeds with both sizes of 32 nm and 20 nm. We have also investigated the effects of other kinetic parameters, including the concentration of reducing agent and reaction temperature, on the growth pathway undertaken by the Au atoms. We believe that the mechanistic insights obtained from this study can be extended to other systems, including the involvement of different metals and/or seeds with different types of internal structures.

INTRODUCTION

Bimetallic nanocrystals have attracted considerable attention in recent years because of their unique properties for a variety of applications in catalysis, electronics, photonics, plasmonics, and surface-enhanced Raman spectroscopy (SERS).[1−7] As a major advantage over their monometallic counterparts, the properties of bimetallic nanocrystals can be engineered by controlling the spatial distributions of the constituent elements.[8−18] Thanks to the efforts from many groups, a variety of bimetallic nanocrystals, including those with a dimeric, dendritic, or core−shell configuration, have been successfully synthesized using solution-phase methods.[19−28] Among these methods, seed-mediated growth, in which newly formed atoms are directed to nucleate and grow from the surface of a preformed seed, has proven to be the most effective, versatile, and reliable approach because the complicated, hard-to-control self-nucleation process can be skipped.[27]

Both the heterogeneous nucleation and growth of atoms on the surface of a seed are sensitive to the reduction kinetics involved in seed-mediated synthesis.[29,30] By manipulating the reduction kinetics, bimetallic nanocrystals with novel structures, including those with an unsymmetric distribution for the constituent elements, have been obtained.[27] In general, the nucleation will be limited to one or a few of the many equivalent sites on the surface of a seed when the reduction of the precursor is kept relatively slow, resulting in the formation of unsymmetric structures. In contrast, when the precursor is reduced at a relatively fast rate, nucleation will be able to occur at all available sites on the surface of a seed, leading to the formation of a core−shell structure. If the reduction is too fast, however, surface diffusion of the adatoms will become inadequate relative to the deposition of atoms and bumps or extruding arms will be formed on the surface.[31] The reduction kinetics of seed-mediated synthesis can be controlled in a number of different ways, including the use of different precursor/reductant combinations and concentrations, as well as the temperature.[32−35] In particular, our group have demonstrated that syringe pump can be used to conveniently manipulate the reduction kinetics of a seed-mediated synthesis and thus obtain nanocrystals (both mono- and bimetallic) with a variety of structures or morphologies.[36] For example, by controlling the injection rate for the precursor solution, the newly formed Ag (or Au) atoms could be directed to selectively nucleate and then epitaxially grow from one to six faces of a Pd cubic seed, leading to the formation of hybrid dimers and non-concentric or concentric core−shell nanocrystals.[8,37]

For single-crystal seeds, the sites available for heterogeneous nucleation and growth are often determined by the types of facets involved, together with the influence of surface capping agents. When switched to seeds with twin defects, one will have another means to manipulate the products as the twin boundaries tend to serve as sites for heterogeneous nucleation and growth due to their surface free energies. As a notable example, Ag, Au, Pd, and Cu penta-twinned nanorods have been synthesized from Au, Pd, or Ag decahedral seeds under a relatively slow reduction for the precursor.[38−42] These examples clearly demonstrate that it is the interplay between the twin defects and reduction kinetics that controls the growth pattern or pathway of a seed.

To gain a better understanding of the interplay between twin defects and reduction kinetics, it would be interesting to explore the use of Pd icosahedra as seeds for the heterogeneous nucleation and growth of another noble metal under controllable reduction kinetics. Although an icosahedron contains 12 vertices and 30 edges lined by twin defects, its surface is less heterogeneous than that of a decahedron, whose surface contains by two different types of vertices and edges.[43] During seed-mediated growth, the newly formed atoms are expected to nucleate from the vertices of an icosahedron and then spread to edges and side faces through surface diffusion. Depending on the reduction kinetics involved, two distinct types of bimetallic nanocrystals are expected to appear: namely, side-by-side dimers and core−shell icosahedra. The present study was focused on the nucleation and growth of Au atoms on Pd icosahedral seeds. The reduction kinetics could be controlled by varying a number of experimental parameters, including the injection rate of $HAuCl_4$ precursor and thus its concentration in the growth solution, the concentration of the reducing agent, and the reaction temperature. At a slow reduction rate, the nucleation of Au atoms was confined to one of the 12 vertices, leading to the formation of a Pd−Au dimeric structure. At a fast reduction rate, in contrast, the Au atoms could nucleate from all 12 vertices and then grown from the entire surface of a Pd icosahedral seed, resulting in the formation of a Pd@Au core−shell icosahedron. The growth pattern was found to exhibit a similar dependence on the reduction kinetics for Pd icosahedral seeds of both 32 nm and 20 nm in size.

EXPERIMENTAL SECTION

Chemicals and Materials. Diethylene glycol (DEG, lot No. BCBK6125V), triethylene glycol (TEG, lot No. BCBJ5292J), poly(vinyl pyrrolidone) (PVP, MW≈55000), gold(III) chloride trihydrate ($HAuCl_4 \cdot 3H_2O$, ≥99.9%), sodium tetrachloropalladate (Na_2PdCl_4, ≥99.9%), aqueous HCl solution (37 wt. % or *ca.* 12 M), and ascorbic acid (AA, ≥99.0%) were all obtained from Sigma-Aldrich and used as received. Deionized (DI) water with a resistivity of 18.2 MΩ·cm was used throughout the experiments.

Synthesis of Pd Icosahedra. For the synthesis of 32-nm Pd icosahedra, 80 mg of PVP was dissolved in 2 mL of DEG in a 20-mL vial and heated in an oil bath at 105 °C for 20 min under magnetic stirring. Meanwhile, another solution was prepared by dissolving 15.5 mg of Na_2PdCl_4 in a mixture of 1 mL of DEG and 2.5 μL of HCl (37%) and then added into the vial in one shot with a pipette. The synthesis was stopped by immersing the vial in an ice-water bath after the reaction had proceeded for 3 h. For the synthesis of 20-nm Pd icosahedra, the procedure was the same as what was used for the 32-nm icosahedra, except that DEG was replaced by TEG and the reaction temperature was increased to 130 °C. The Pd icosahedra were collected by centrifugation at 10,000 rpm for 15 min and washed with acetone and DI water, and finally redispersed in 3 mL of DI water for further use or storage.

Synthesis of Pd−Au Bimetallic Nanocrystals. For the standard procedure, 5.4 mL of an aqueous suspension containing the as-prepared 32-nm Pd icosahedra (0.33 mM in terms of elemental Pd), AA (0.37 mM), and PVP (3.3 mM) were mixed in a 20-mL vial. The mixture was held at room temperature for 20 min under magnetic stirring. Meanwhile, 2 mL of an aqueous $HAuCl_4$ solution (0.5 mM) was freshly prepared at room temperature and injected into the vial at a controlled rate. In all cases, the reaction solution was maintained under magnetic stirring for another 10 min after all the $HAuCl_4$ solution had been injected to allow the reaction to complete. The product was collected by centrifugation at 10,000 rpm for 15 min and washed with water three times.

Instrumentation. Transmission electron microscopy (TEM) images were obtained using a Hitachi H-7500 microscope operated at 75 kV. High-resolution TEM images, high-angle annular dark-field scanning TEM (HAADF-STEM) images, and energy dispersive X-ray (EDX)

mapping were acquired using a double Cs-corrected JEOL ARM200F TEM at Brookhaven National Laboratory. An Eppendorf centrifuge (5430) was used for the centrifugation and washing of all samples.

RESULTS AND DISCUSSION

We used a syringe pump to control the introduction of an aqueous $HAuCl_4$ solution into an aqueous mixture containing Pd icosahedral seeds, AA, and PVP under magnetic stirring at room temperature. By varying the injection rate and other reaction parameters, such as the concentration of AA and the reaction temperature, we could maneuver the growth mode undertaken by Au atoms when they were deposited onto the Pd icosahedral seeds. Figure 1 shows TEM images of Pd icosahedral seeds and the Pd−Au bimetallic nanocrystals obtained with different injection rates for the $HAuCl_4$ solution. Specifically, Figure 1a shows a TEM image and the corresponding three-dimensional (3D) model of the Pd icosahedral seeds with an average size (defined as the distance between two opposite faces) of 32 nm. Figure 1, b−d, shows TEM images and the corresponding 3D models of the Pd−Au bimetallic nanocrystals obtained after the introduction of 2 mL of $HAuCl_4$ solution in different ways. At a relatively slow injection rate of 0.2 mL h^{-1} (Figure 1b), the nucleation and growth of Au atoms were confined to five adjacent twin boundaries on a Pd icosahedral seed, resulting in the formation of a Pd−Au dimer. In this case, the Au portion also took an icosahedral structure by sharing five of its faces with the Pd icosahedral seed. The growth pattern was similar to what was observed in our previous study, where a Pd−Au hybrid dimer was formed through the nucleation and growth of Au atoms from one of the six faces of a Pd cubic seed at a relatively slow injecting rate.[37]

When the injection rate of the $HAuCl_4$ precursor was increased from 0.2 to 0.5 mL h^{-1} while all other parameters were kept the same, the concentration of Au atoms around each Pd seed was increased to a level high enough to facilitate nucleation and growth from the entire surface of a Pd seed, resulting in the formation of a Pd@Au core−shell icosahedron (Figure 1c). Similarly, when the $HAuCl_4$ solution was added into the reaction mixture in one shot, we also obtained Pd@Au core−shell nanocrystals, but with a rough surface (Figure 1d), owing to the uneven deposition of Au atoms along different directions of a seed.

We then used HAADF-STEM, HRTEM, and EDX elemental mapping to fully characterize

the structure and composition of the Pd−Au bimetallic nanocrystals. The HAADF-STEM image in Figure 2a shows clear contrast between the Pd and Au portions arranged side by side, confirming the formation of a Pd−Au dimeric structure. The elemental distributions of an individual Pd−Au dimer were revealed by line scan profiles, HAADF-STEM, and EDX mapping in Figure 2, b−e. Distinct Au signal was detected from one side, while the Pd signal was observed from the other side, confirming the formation of a Pd−Au side-by-side dimeric structure.

The HAADF-STEM image in Figure 3a confirms the formation of a Pd@Au core−shell structure. The magnified HAADF-STEM image in the inset of Figure 3b shows a perfect core−shell structure with a uniform shell thickness of *ca.* 4 nm. The elemental distributions of a single Pd@Au core−shell icosahedron were confirmed by line scan profiles, HAADF-STEM, and EDX mapping shown in Figure 3, b−e. The EDX mapping clearly show a difference in color between the interior (green, mainly Pd) and the outer layer (red, mainly Au), confirming the formation of a bimetallic core−shell structure.

In order to resolve the detail steps involved in the growth of Pd−Au icosahedral dimers, we conducted a set of experiments by varying the volume of $HAuCl_4$ solution added into the growth solution. Figure 4 shows TEM images and the corresponding 3D models of the Pd−Au dimeric nanocrystals obtained. When a smaller volume of $HAuCl_4$ solution was added into the reaction solution (0.25 mL *vs.* 2 mL) while all other conditions were kept the same as in Figure 1b, the Au atoms were only able to nucleate from one of the twelve vertices of a Pd icosahedral seed due to the limited supply of precursor (Figure 4a). The heterogeneous nucleation took place from a vertex rather than an edge or a side face simply because of the highest surface free energy at the vertex site. When the volume of $HAuCl_4$ solution was increased to 0.75 mL, some of the newly generated Au atoms were spread from the vertex site to one of its adjacent side faces, generating a Pd−Au dimer with a partially developed Au tetrahedron (Figure 4b). As the volume of $HAuCl_4$ solution was increased to 1.0 mL, four Au tetrahedral particles were formed by sharing two adjacent faces of a Pd icosahedral seed (Figure 4c). When the volume of $HAuCl_4$ solution reached 1.5 mL, the number of Au tetrahedral units increased to more than 8 and these Au tetrahedral units shared three or four adjacent faces of a Pd icosahedral seed (Figure 4d). Finally, at a volume of 2.0 mL for the $HAuCl_4$ solution, an icosahedral structure was fully developed for the Au component by sharing five faces with the Pd icosahedral seed (Figure 1b).

In addition to the injection rate, the concentration of AA was also found to play a critical role in controlling the reduction rate of $HAuCl_4$ during the formation of Pd−Au nanocrystals. Figure 5 shows typical TEM images of the products obtained at different concentrations of AA while the injection rate was set to 0.5 mL h^{-1} for the $HAuCl_4$ solution. At a relatively low concentration of AA (0.28 mM), the number of Au atoms derived from the reduction of $HAuCl_4$ stayed at a low level around each Pd seed. These Au atoms were unable to initiate multiple nucleation sites on a Pd seed. Typically, only one of the twelve vertices was involved in the heterogeneous nucleation process, leading to the formation of Pd−Au bimetallic dimers (Figure 5a). When the concentration of AA was increased to 0.37 mM, there were adequate Au atoms in the solution to ensure multiple nucleation sites on each Pd seed, and thereby the formation of Pd@Au core−shell nanocrystals (Figure 1c). When the concentration of AA was increased to 1.11 mM, the number of Au atoms would be large enough to generate multiple nucleation sites on each Pd seed while the diffusion rate of Au adatoms would not change. As a result, Pd@Au core−shell nanocrystals with a rough surface were formed (Figure 5b). These results indicate that the nucleation and growth of Au on a Pd icosahedral seed was highly sensitive to the concentration of AA. It is a combination of the $HAuCl_4$ injection rate and the concentration of AA that determines the deposition rate of Au atoms onto each Pd seed, and thus the growth pattern.

We also investigated the role of reducing agent in the formation of Pd−Au nanocrystals by injecting the $HAuCl_4$ solution in one shot. Figure S1 shows the typical TEM images of products obtained at different concentrations of AA while all other conditions were kept the same as in Figure 1d. When the concentration of AA was relatively low (0.28 mM), Pd−Au bimetallic dimers were obtained (Figure S1a). In this case, Au atoms mainly nucleated and grew from fewer than five of the twenty faces of a Pd icosahedral seed, similar to the Pd−Au bimetallic nanocrystals obtained at the same concentration of AA but at a lower injection rate for the $HAuCl_4$ solution (0.5 mL h^{-1}, Figure 5a). When the reduction kinetics was speeded up by increasing the concentration of AA to 1.11 mM, the resultant Au atoms would nucleate and grow from the entire surface of a Pd icosahedral seed, resulting in the formation of Pd@Au core−shell nanocrystals with a rough surface (Figure S1b). Different from the case shown in Figure 1d, however, some Au nanoparticles were also formed through homogeneous nucleation due to the high concentration of AA and thus a much accelerated reduction rate.

Reaction temperature is also an important parameter to examine because it directly controls the reduction rate and surface diffusion rate and thus the shape of the final products.[31] Figure 6 shows TEM images of Pd−Au bimetallic nanocrystals obtained at different reaction temperatures, with all the other parameters being kept the same as in Figure 1b. At a relatively low temperature of 0 °C, Au bumps (one or a few) were formed on each Pd icosahedral seed and the Au particles were dominated by either a partial icosahedral or plate-like morphology (Figure 6a). In contrast, when the temperature was increased to 40 °C, a mixture of Pd−Au bimetallic dimers and Pd@Au core−shell nanocrystals was obtained due to the enhancement in surface diffusion (Figure 6b). At 60 °C, the surface diffusion of Au atoms was further accelerated, leading to the formation of Pd@Au core−shell icosahedra (Figure 6c). These results suggest that the reaction temperature plays a critical role in the formation of Pd−Au bimetallic nanocrystals with different morphologies. In general, a higher reaction temperature would speed up the surface diffusion of Au adatoms to facilitate the formation of Pd@Au core−shell nanocrystals.

Finally, we also extended the same research to Pd icosahedral seeds with a much smaller size of 20 nm. In this case, we conducted a set of experiments by replacing the 32-nm Pd icosahedra with 20-nm Pd icosahedra while all other experimental parameters were kept the same as in Figure 1. Figure S2a shows a TEM image of the as-prepared Pd icosahedral seeds with an average size of 20 nm. At a relatively low injection rate of 0.2 mL h^{-1} for the $HAuCl_4$ solution, Pd−Au dimers were also obtained (Figure S2b). Different from the dimers obtained using 32-nm Pd icosahedral seeds, the Au portion shared more than five faces with the Pd icosahedral seed due to the spreading of Au atoms through surface migration. Increasing the injection rate of $HAuCl_4$ precursor from 0.2 to 0.5 mL h^{-1} while keeping other conditions the same, Pd@Au core−shell spheres were obtained (Figure S2c). Apparently, the surface diffusion of Au atoms was able to cover the entire surface of a Pd seed because of the reduced length scale. When the $HAuCl_4$ precursor was introduced in one shot, Pd@Au core−shell nanocrystals with a rough surface and discrete Au nanoparticles were obtained due to the involvement of both heterogeneous and homogeneous nucleation (Figure S2d).

CONCLUSION

In summary, we have successfully controlled the growth of Au on a Pd icosahedral seed by

manipulating the reduction kinetics. By varying a set of experimental parameters, including the injection rate of the Au precursor solution, the concentration of reducing agent, and reduction temperature, two types of Pd−Au bimetallic nanocrystals were obtained corresponding to different reduction rates. At a fast reduction rate, the Au atoms could nucleate and grow from the entire surface of a Pd icosahedral seed, leading to the formation of a Pd@Au core−shell nanocrystal. In contrast, the Au atoms preferentially nucleated and grew from the one of the vertices of a Pd icosahedral seed at a relatively slow reduction rate, resulting in the formation of a Pd−Au dimer. We have validated the growth patterns using Pd icosahedral seeds with two different sizes of 20 nm and 32 nm. We believe the mechanistic understanding obtained in this work can also be extended to other combinations of noble metals, as well as seeds with different internal structures.

AUTHOR INFORMATION

Corresponding Author

*younan.xia@bme.gatech.edu

Notes

The authors declare no competing financial interest.

ACKNOWLEDGMENT

This work was supported in part by a grant from NSF (CHE-1505441) and startup funds from the Georgia Institute of Technology. The electron microscopy analysis at BNL was supported by the U.S. Department of Energy, Basic Energy Sciences, through the Materials Sciences and Engineering Division under Contract No. DE-AC02-98CH10886. As visiting Ph.D. students from East China Normal University and Xiamen University, respectively, T.L. and L.Z. were both partially supported by the China Scholarship Council (CSC).

REFERENCES

[1] Rodriguez, J. A.; Goodman, D. W. The Nature of the Metal-Metal Bond in Bimetallic Surfaces. *Science* **1992**, *257*, 897−903.

[2] Link, S.; Wang, Z. L.; El-Sayed, M. A. Alloy Formation of Gold-Silver Nanoparticles and the Dependence of the Plasmon Absorption on Their Composition. *J. Phys. Chem. B* **1999**, *103*, 3529−3533.

[3] Xia, Y.; Xiong, Y.; Lim, B.; Skrabalak, S. E. Shape-Controlled Synthesis of Metal Nanocrystals: Simple Chemistry Meets Complex Physics? *Angew. Chem., Int. Ed*. **2009**, *48*, 60−103.

[4] Wang, D.; Li, Y. Bimetallic Nanocrystals: Liquid-Phase Synthesis and Catalytic Applications. *Adv. Mater*. **2011**, *23*, 1044−1060.

[5] Yang, H. Platinum-Based Electrocatalysts with Core-Shell Nanostructures. *Angew. Chem., Int. Ed*. **2011**, *50*, 2674−2676.

[6] Peng, Z.; Yang, H. Designer Platinum Nanoparticles: Control of Shape, Composition in Alloy, Nanostructure and Electrocatalytic Property. *Nano Today* **2009**, *4*, 143−164.

[7] Tao, A. R.; Habas, S.; Yang, P. Shape Control of Colloidal Metal Nanocrystals. *Small* **2008**, *4*, 310−325.

[8] Zeng, J.; Zhu, C.; Tao, J.; Jin, M.; Zhang, H.; Li, Z.-Y.; Zhu, Y.; Xia, Y. Controlling the Nucleation and Growth of Silver on Palladium Nanocubes by Manipulating the Reaction Kinetics. *Angew. Chem., Int. Ed*. **2012**, *51*, 2354−2358.

[9] He, G.; Zeng, J.; Jin, M.; Zhang, H.; Lu, N.; Wang, J.; Kim, M. J.; Xia, Y. A Mechanistic Study on the Nucleation and Growth of Au on Pd Seeds with a Cubic or Octahedral Shape. *ChemCatChem* **2012**, *4*, 1668−1674.

[10] Zhang, J.; Vukmirovic, M. B.; Xu, Y.; Mavrikakis, M.; Adzic, R. R. Controlling the Catalytic Activity of Platinum-Monolayer Electrocatalysts for Oxygen Reduction with Different Substrates. *Angew. Chem., Int. Ed*. **2005**, *44*, 2132−2135.

[11] Lim, B.; Wang, J.; Camargo, P. H. C.; Jiang, M.; Kim, M. J.; Xia, Y. Facile Synthesis of Bimetallic Nanoplates Consisting of Pd Cores and Pt Shells through Seeded Epitaxial Growth. *Nano Lett*. **2008**, *8*, 2535−2540.

[12] Zhou, S.; McIlwrath, K.; Jackson, G.; Eichhorn, B. Enhanced CO Tolerance for Hydrogen Activation in Au-Pt Dendritic Heteroaggregate Nanostructures. *J. Am. Chem. Soc.* **2006**,

128, 1780−1781.

[13] Peng, Z.; Yang, H. Synthesis and Oxygen Reduction Electrocatalytic Property of Pt-on-Pd Bimetallic Heteronanostructures. *J. Am. Chem. Soc.* **2009**, *131*, 7542−7543.

[14] Lim, B.; Jiang, M.; Yu, T.; Camargo, P. H. C.; Xia, Y. Nucleation and Growth Mechanisms for Pd-Pt Bimetallic Nanodendrites and Their Electrocatalytic Properties. *Nano Res*. **2010**, *3*, 69−80.

[15] Min, M.; Kim, C.; Yang, Y. I.; Yi, J.; Lee, H. Surface-Specific Overgrowth of Platinum on Shaped Gold Nanocrystals. *Phys. Chem. Chem. Phys*. **2009**, *11*, 9759−9765.

[16] Lim, B.; Jiang, M.; Camargo, P. H. C.; Cho, E. C.; Tao, J.; Lu, X.; Zhu, Y.; Xia, Y. Pd-Pt Bimetallic Nanodendrites with High Activity for Oxygen Reduction. *Science* **2009**, *324*, 1302−1305.

[17] Lim, B.; Kobayashi, H.; Yu, T.; Wang, J.; Kim, M. J.; Li, Z.-Y.; Rycenga, M.; Xia, Y. Synthesis of Pd-Au Bimetallic Nanocrystals via Controlled Overgrowth. *J. Am. Chem. Soc*. **2010**, *132*, 2506−2507.

[18] Lu, C.-L.; Prasad, K. S.; Wu, H.-L.; Ho, J.-a. A.; Huang, M. H. Au Nanocube-Directed Fabrication of Au-Pd Core-Shell Nanocrystals with Tetrahexahedral, Concave Octahedral, and Octahedral Structures and Their Electrocatalytic Activity. *J. Am. Chem. Soc*. **2010**, *132*, 14546−14553.

[19] Hu, J.-W.; Zhang, Y.; Li, J.-F.; Liu, Z.; Ren, B.; Sun, S.-G.; Tian, Z.-Q.; Lian, T. Synthesis of Au@Pd Core-Shell Nanoparticles with Controlled Size and Their Application in Surface-Enhanced Raman Spectroscopy. *Chem. Phys. Lett*. **2005**, *408*, 354−359.

[20] Xiang, Y.; Wu, X.; Liu, D.; Jiang, X.; Chu, W.; Li, Z.; Ma, Y.; Zhou, W.; Xie, S. Formation of Rectangularly Shaped Pd/Au Bimetallic Nanorods: Evidence for Competing Growth of the Pd Shell between the {110} and {100} Side Facets of Au Nanorods. *Nano Lett*. **2006**, *6*, 2290−2294.

[21] Fan, F.-R.; Liu, D.-Y.; Wu, Y.-F.; Duan, S.; Xie, Z.-X.; Jiang, Z.-Y.; Tian, Z.-Q. Epitaxial Growth of Heterogeneous Metal Nanocrystals: From Gold Nano-octahedra to Palladium and Silver Nanocubes. *J. Am. Chem. Soc*. **2008**, *130*, 6949−6951.

[22] Lee, Y. W.; Kim, M.; Kang, S. W.; Han, S. W. Polyhedral Bimetallic Alloy Nanocrystals Exclusively Bound by {110} Facets: Au-Pd Rhombic Dodecahedra. *Angew. Chem., Int. Ed*. **2011**, *50*, 3466−3470.

[23] Yang, C.-W.; Chanda, K.; Lin, P.-H.; Wang, Y.-N.; Liao, C.-W.; Huang, M. H. Fabrication of Au-Pd Core-Shell Heterostructures with Systematic Shape Evolution Using Octahedral Nanocrystal Cores and Their Catalytic Activity. *J. Am. Chem. Soc*. **2011**, *133*, 19993−20000.

[24] Zhang, H.; Jin, M.; Wang, J.; Li, W.; Camargo, P. H. C.; Kim, M. J.; Yang, D.; Xie, Z.; Xia, Y. Synthesis of Pd-Pt Bimetallic Nanocrystals with a Concave Structure through a Bromide-Induced Galvanic Replacement Reaction. *J. Am. Chem. Soc*. **2011**, *133*, 6078−6089.

[25] Li, J.; Zheng, Y.; Zeng, J.; Xia, Y. Controlling the Size and Morphology of Au@Pd Core-Shell Nanocrystals by Manipulating the Kinetics of Seeded Growth. *Chem. Eur. J*. **2012**, *18*, 8150−8156.

[26] Gong, J.; Zhou, F.; Li, Z.; Tang, Z. Controlled Synthesis of Non-Epitaxially Grown Pd@Ag Core-Shell Nanocrystals of Interesting Optical Performance. *Chem. Commun*. **2013**, *49*, 4379−4381.

[27] Xia, Y.; Xia, X.; Peng, H.-C. Shape-Controlled Synthesis of Colloidal Metal Nanocrystals: Thermodynamic versus Kinetic Product. *J. Am. Chem. Soc.* **2015**, *137*, 7947−7966.

[28] Niu, W.; Zhang, L.; Xu, G. Seed-Mediated Growth of Noble Metal Nanocrystals: Crystal Growth and Shape Control. *Nanoscale* **2013**, *5*, 3172−3181.

[29] Xia, X.; Choi, S.-I.; Herron, J. A.; Lu, N.; Scaranto, J.; Peng, H.-C.; Wang, J.; Mavrikakis, M.; Kim, M. J.; Xia, Y. Facile Synthesis of Palladium Right Bipyramids and Their Use as Seeds for Overgrowth and as Catalysts for Formic Acid Oxidation. *J. Am. Chem. Soc.* **2013**, *135*, 15706−15709.

[30] Peng, H.-C.; Park, J.; Zhang, L.; Xia, Y. Toward a Quantitative Understanding of Symmetry Reduction Involved in the Seed-Mediated Growth of Pd Nanocrystals. *J. Am. Chem. Soc.* **2015**, *137*, 6643−6652.

[31] Xia, X.; Xie, S.; Liu, M.; Peng, H.-C.; Lu, N.; Wang, J.; Kim. M. J.; Xia, Y. On the Role of Surface Diffusion in Determining the Shape or Morphology of Noble-Metal Nanocrystals. *Proc. Natl. Acad. Sci. USA* **2013**, *110*, 6669−6673.

[32] Xie, S.; Choi, S.-I.; Lu, N.; Roling, L. T.; Herron, J. A.; Zhang, L.; Park, J.; Wang, J.; Kim, M. J.; Xie, Z. et al. Atomic Layer-by-Layer Deposition of Pt on Pd Nanocubes for Catalysts with Enhanced Activity and Durability toward Oxygen Reduction. *Nano Lett.*

2014, *14*, 3570−3576.

[33] Park, J.; Zhang, L.; Choi, S.-I.; Roling, L. T.; Lu, N.; Herron, J. A.; Xie, S.; Wang, J.; Kim, M. J.; Mavrikakis, M. et al. Atomic Layer-by-Layer Deposition of Platinum on Palladium Octahedra for Enhanced Catalysts toward the Oxygen Reduction Reaction. *ACS Nano* **2015**, *9*, 2635−2647.

[34] Wang, X.; Choi, S.-I.; Roling, L. T.; Luo, M.; Ma, C.; Zhang, L.; Chi, M.; Liu, J.; Xie, Z.; Herron, J. A. et al. Palladium−Platinum Core−Shell Icosahedra with Substantially Enhanced Activity and Durability towards Oxygen Reduction. *Nat. Commun.* **2015**, *6*, 7594.

[35] Wang, X.; Vara, M.; Luo, M.; Huang, H.; Ruditskiy, A.; Park, J.; Bao, S.; Liu, J.; Howe, J.; Chi, M. et al. Pd@Pt Core−Shell Concave Decahedra: A Class of Catalysts for the Oxygen Reduction Reaction with Enhanced Activity and Durability. *J. Am. Chem. Soc.* **2015**, *137*, 15036−15042.

[36] Zhang, H.; Li, W.; Jin, M.; Zeng, J.; Yu, T.; Yang, D.; Xia, Y. Controlling the Morphology of Rhodium Nanocrystals by Manipulating the Growth Kinetics with a Syringe Pump. *Nano Lett*. **2011**, *11*, 898−903.

[37] Zhu, C.; Zeng, J.; Tao, J.; Johnson, M. C.; Schmidt-Krey, I.; Blubaugh, L.; Zhu, Y.; Gu, Z.; Xia, Y. Kinetically Controlled Overgrowth of Ag or Au on Pd Nanocrystal Seeds: from Hybrid Dimers to Nonconcentric and Concentric Bimetallic Nanocrystals. *J. Am. Chem. Soc*. **2012**, *134*, 15822−15831.

[38] Langille, M. R.; Zhang, J.; Mirkin, C. A. Plasmon-Mediated Synthesis of Heterometallic Nanorods and Icosahedra. *Angew. Chem., Int. Ed*. **2011**, *50*, 3543−3547.

[39] Pietrobon, B.; McEachran, M.; Kitaev, V. Synthesis of Size-Controlled Faceted Pentagonal Silver Nanorods with Tunable Plasmonic Properties and Self-Assembly of These Nanorods. *ACS Nano* **2009**, *3*, 21−26.

[40] Yang, Y.; Wang, W.; Li, X.; Chen, W.; Fan, N.; Zou, C.; Chen, X.; Xu, X.; Zhang, L.; Huang, S. Controlled Growth of Ag/Au Bimetallic Nanorods through Kinetics Control. *Chem. Mater.* **2013**, *25*, 34−41.

[41] Luo, M.; Huang, H.; Choi, S.-I.; Zhang, C.; da Silva, R. R.; Peng, H.-C.; Li, Z.-Y.; Liu, J.; He, Z.; Xia, Y. Facile Synthesis of Ag Nanorods with No Plasmon Resonance Peak in the Visible Region by Using Pd Decahedra of 16 nm in Size as Seeds. *ACS Nano* **2015**, *9*,

10523−10532.

[42] Luo, M.; Ruditskiy, A.; Peng, H.-C.; Tao, J.; Figueroa-Cosme, L.; He, Z.; Xia, Y. Penta-Twinned Copper Nanorods: Facile Synthesis via Seed-Mediated Growth and Their Tunable Plasmonic Properties. *Adv. Funct. Mater.* **2016**, *26*, 1209−1216.

[43] Xiong, Y.; McLellan, J. M.; Yin, Y.; Xia, Y. Synthesis of Palladium Icosahedra with Twinned Structure by Blocking Oxidative Etching with Citric Acid or Citrate Ions. *Angew. Chem., Int. Ed*. **2007**, *46*, 790−794.

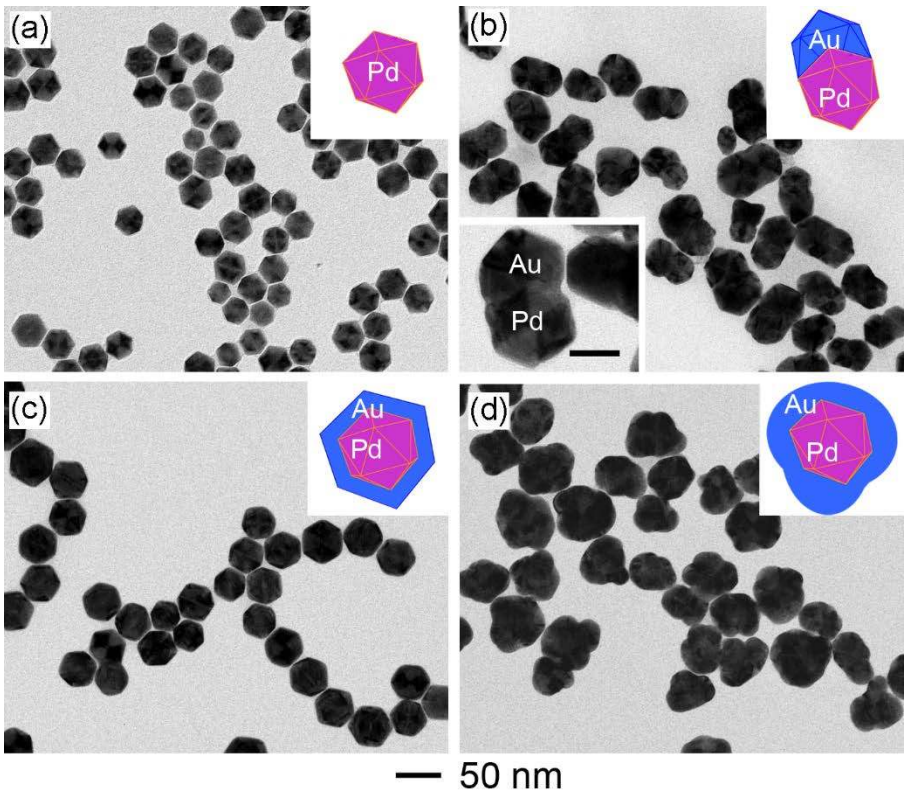

Figure 1. (a) TEM images of the 32-nm Pd icosahedral seeds and (b−d) the Pd−Au bimetallic nanocrystals obtained by injecting the aqueous $HAuCl_4$ solution at different rates: (b) 0.2 mL h^{-1}, (c) 0.5 mL h^{-1}, and (d) one shot. The scale bar in the inset of (b) is 20 nm. The inset in the up-right corner shows a 3D model of the corresponding nanocrystal.

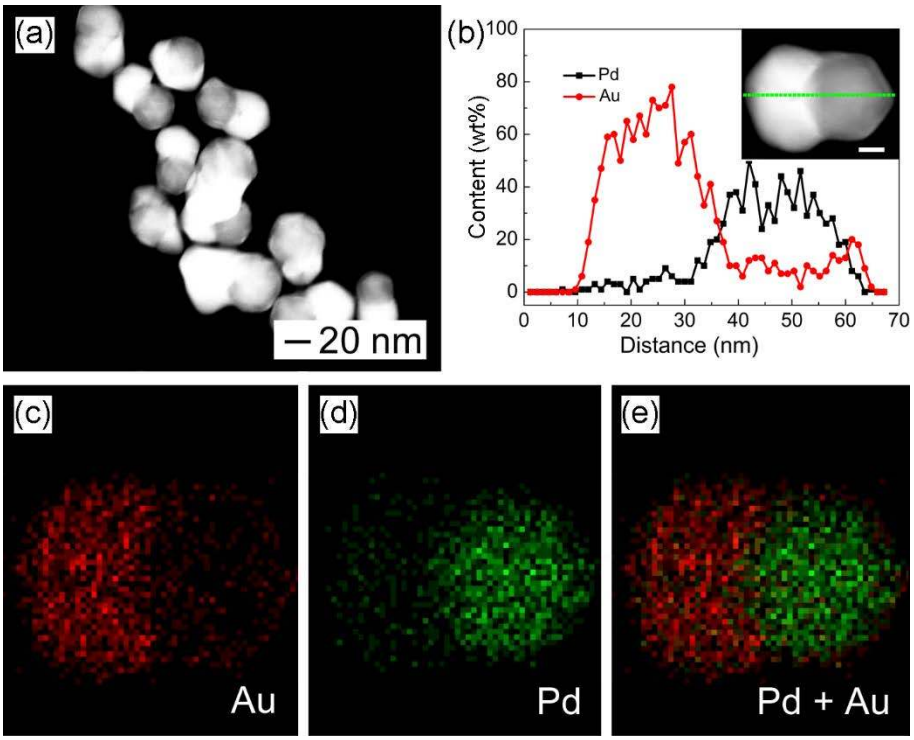

Figure 2. Structural characterizations of the Pd−Au dimeric nanocrystals obtained by injecting the $HAuCl_4$ solution at a rate of 0.2 mL h^{-1}: (a) HAADF-STEM image; (b) line scan profiles of a single Pd−Au dimer along the dashed line; and (c−e) EDX elemental mapping. The inset of (b) is a HAADF-STEM image for one particle.

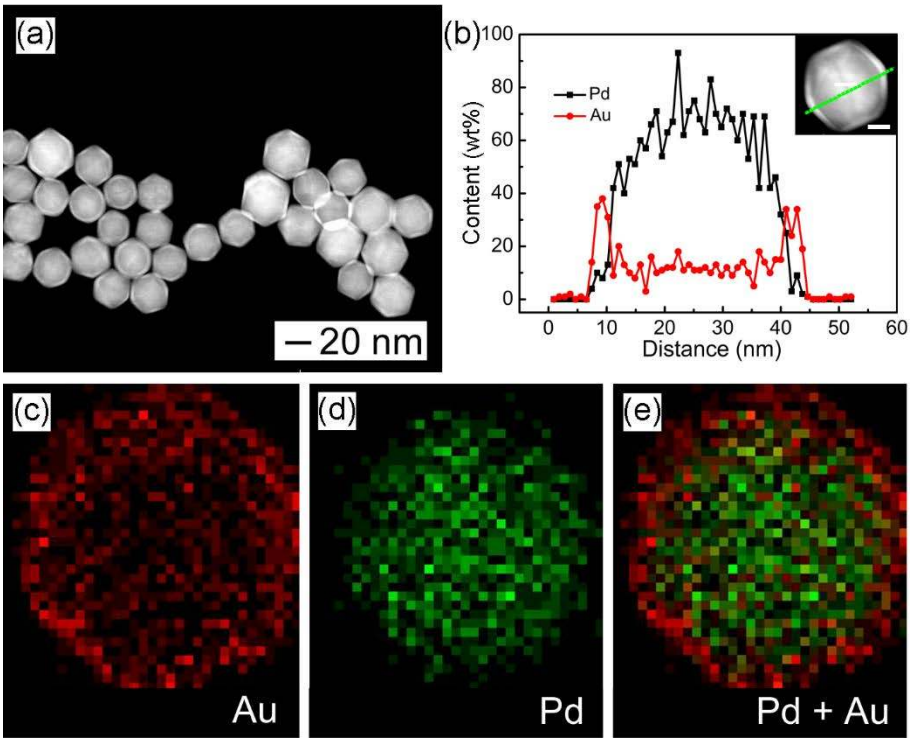

Figure 3. Structural characterizations of the Pd@Au core−shell nanocrystals obtained by injecting the $HAuCl_4$ solution at a rate of 0.5 mL h^{-1}: (a) HAADF-STEM image; (b) line scan profiles of a single Pd@Au core−shell icosahedron along the dashed line; and (c−e) EDX elemental mapping. The inset of (b) is a HAADF-STEM image for one particle.

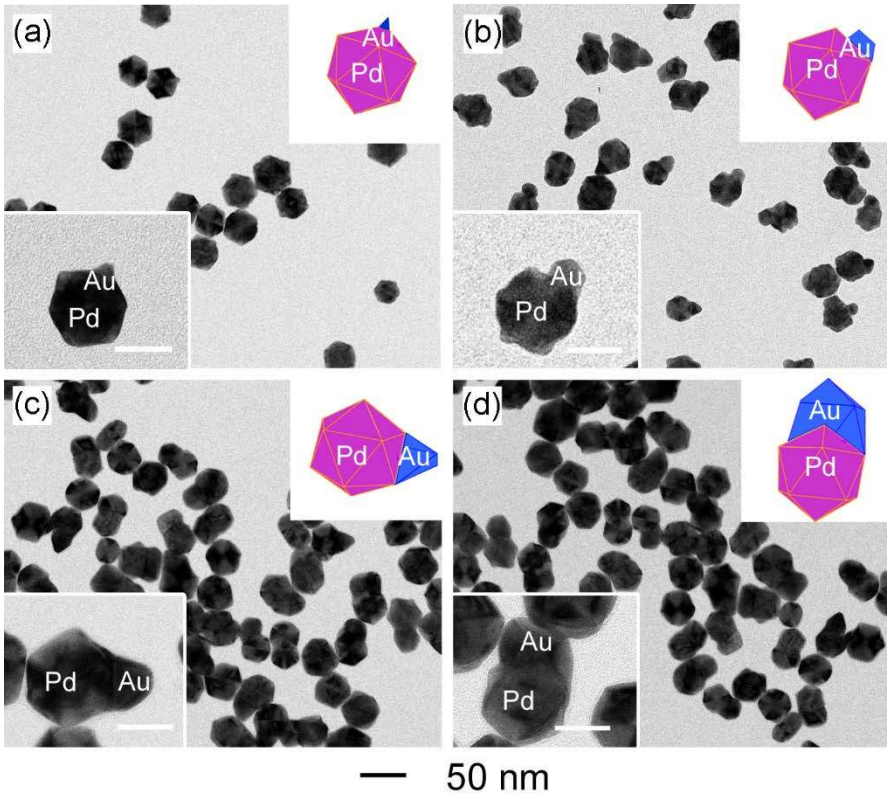

Figure 4. TEM images of Pd−Au bimetallic nanocrystals obtained by injecting the $HAuCl_4$ solution at a rate of 0.2 mL h^{-1}. The total volumes of the added $HAuCl_4$ solution were: (a) 0.25, (b) 0.75, (c) 1.0, and (d) 1.5 mL. The scale bars in the insets are 20 nm. The inset at the up-right corner shows a 3D model of the corresponding nanocrystal.

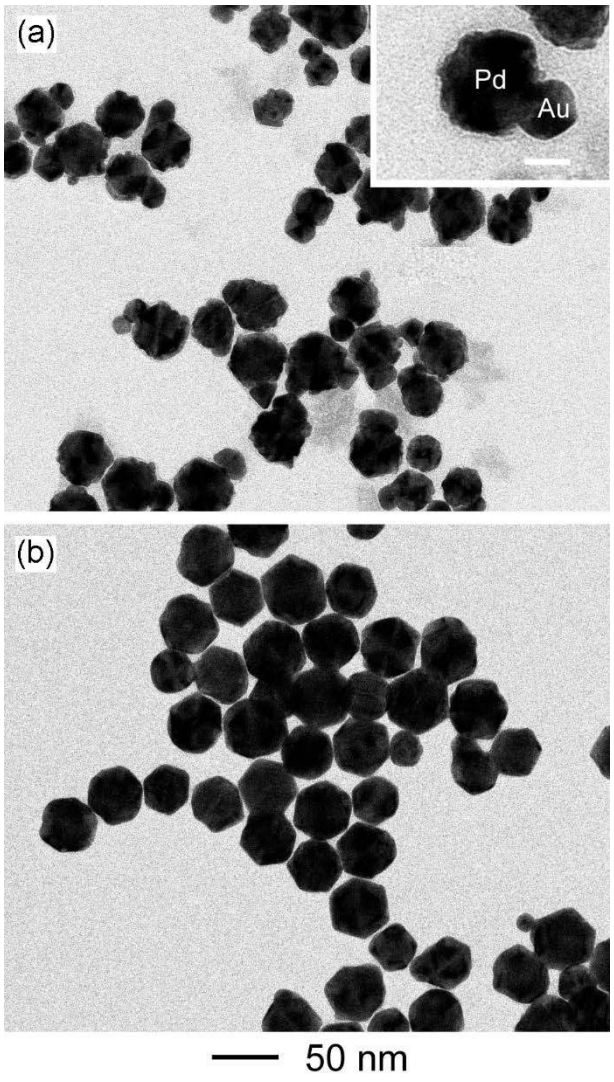

Figure 5. TEM images of Pd−Au bimetallic nanocrystals obtained in the presence of AA at two different concentrations: (a) 0.28 and (b) 1.11 mM, respectively. The injection rate for the $HAuCl_4$ solution was kept at 0.5 mL h^{-1}. The scale bar in the inset of (a) is 20 nm.

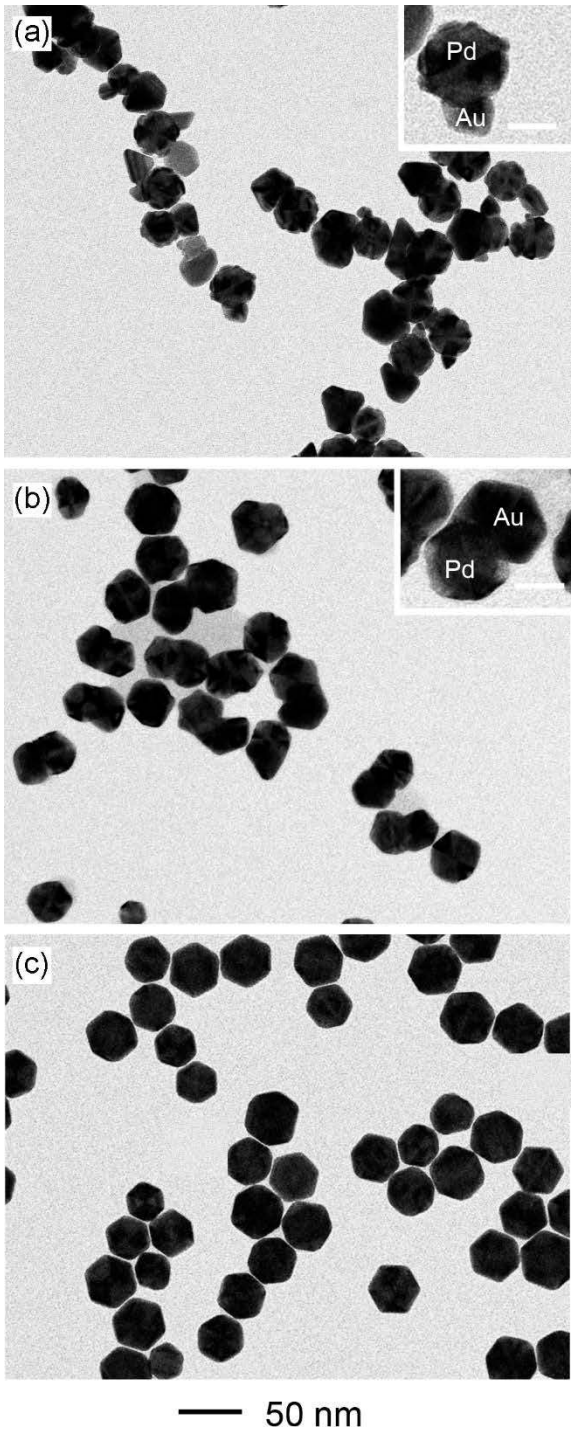

Figure 6. TEM images of nanocrystals obtained by injecting 2 mL of the $HAuCl_4$ solution at 0.2 mL h^{-1} while the solution was set to different temperatures: (a) 0, (b) 40, and (c) 60 °C. The concentration of AA was 0.37 mM. The scale bars in the insets are 20 nm.

TOC